MO Calculation for the Oxygen Interacting with Ni24(100) Model Surface

Kwang-Soon Lee†, Hyun-Joo Koo, Yoon Chang Park, and Woon-Sun Ahn*

Department of Chemistry, Sung Kyun Kwan University, Suwon 440-746
†Department of Chemistry, Song Sim University, Puchon 422-743
Received September 10, 1993

The DOS, COOP and O 1s binding energy are calculated for Ni24(100) model surface with oxygen adsorbed on it. The calculation is made with PC/386 using the program obtained by converting EHMACC(VAX version) into PC version. The calculation shows the dissociative adsorption of oxygen molecule, of which the main cause is attributed to the transfer of the $d\pi$ and $d\delta$ electrons of Ni to the antibonding $1\pi_g$ of oxygen molecule. The O 1s shift on the adsorption is calculated using the valence potential method, and the results agree fairly good with the experimental values.

Introduction

The interaction between oxygen (from the gas phase) and nickel surface, such as the identification of the adsorbed oxygen species, adsorption sites of the surface, geometrical structure formed by adsorbed species and Ni-O bond strength, have been the very interesting subjects for those working on the catalytic activity, corrosion, passivity of transition metals, and etc.

Bielanski *et al.*[1] and Dyrek[2] studied oxygen species adsorbed on a nickel surface with EPR and concluded that the oxygen is adsorbed to form O^- or O_2^-. Tsyganenko *et al.*[3] also studied the oxygen on NiO surface with IR and found an evidence of O_2^- species formation. Hedge *et al.*[4] asserted that oxygen is dissociatively adsorbed on nickel surface to take a non-integral oxidation state between O^- and O^{2-}. Meanwhile, the X-ray photoelectron spectra of oxygen adsorbed on nickel support invariably the evidence of the dissociatively adsorbed species only, although their 1s binding energy shows several peaks corresponding to varying degree of oxidation.[5-8] A peak at 531.3 eV among these peaks is especially dubious. Some attribute this peak to Ni_2O_3 oxygen while Ahn *et al.*[8] attribute it to nonstoichiometrical excess oxygen on the surface NiO. Arnaud *et al.*[9] found several desorption peaks of oxygen on the temperature programmed desorption spectrum of nickel oxide, and attributed it to the different coordination numbers the oxygen atom takes on the surface and in the bulk.

The geometrical structure is another important factor in considering the interaction of oxygen with the nickel (100) surface. Stöhr *et al.*[10] studied the same system with SEXAFS and found that the oxygen atom occupies 4-fold site of the surface to form the $p(2\times2)$ structure at 1.5 L exposure and the $c(2\times2)$ structure at 20-30L exposure. Preceding to this finding, Rahman[11] found using EELS that the adsorbed oxygen atom interacts with the 4 nearest neighbour Ni atoms only, and that the Ni-O bond in the $c(2\times2)$ structure is shorter than the one in the $p(2\times2)$ structure. Antognangeli *et al.*[12] found with SEELFS experiments the generation of NiO islands at an oxygen coverage of 0.7 preceded by the $c(2\times2)$ structure formation at low coverage of oxygen.

The studies of interaction between oxygen and nickel surface may lead to diverse interpretations depending on the experimental instruments and the methods as outlined above. Theoretical consideration based on MO calculation can be a great help in interpreting as well as understanding the experimental results as a whole. Anderson *et al.*[13] applied the extended Hückel MO theory, to the surface adsorption, and Blyholder[14], using the Hückel MO theory, interpreted successfully the IR spectrum of CO chemisorbed on the metal surface. Hoffmann, Whangbo and their coworkers[15-18] applied the band theory in interpreting the interaction between adsorbate species and the metal surface.

In the first part of this work, the energy band, density of state (DOS), and crystal orbital overlap population (COOP) for an Ni24(100) surface are calculated using the method developed by Hoffmann, Whangbo *et al.*[19-21] These calculations are applied further to the exploration of the dissociative adsorption of oxygen molecules on the model surface. In the latter part, the interaction between the adsorbed species and the model surface is studied to estimate the O 1s binding energy shift upon the adsorption.

Theories

Dissociative Adsorption. It has been known that a model of at least 20 metal atoms is necessary in order to study the interaction of metallic crystal surface to an adsorbate gas molecule theoretically.[22] A model surface of 24 nickel atoms are used to represent the (100) surface in this work in order to consider the symmetry of the surface as shown in Figure 1.

The band structure of the model surface is then calculated with the tight-binding extended Hückel theory applied to a unit cell of the model surface using the boundary conditions of the corresponding Brillouin zone. The double zeta function is used for the atomic orbitals, of which the parameters are given in the Appendix. The DOS of the calculated band structure is smoothed out to the following gaussian function.[23]

$$\mathrm{DOS}=\sum_{i=1}^{M\times L} 2g_i(\epsilon) \qquad (1)$$

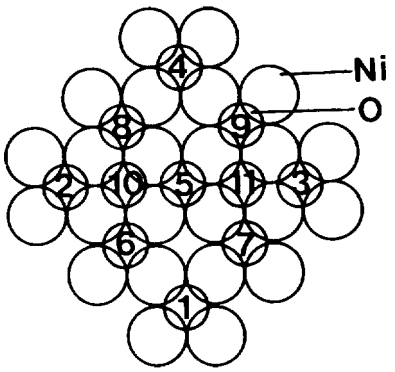

Figure 1. Ni24(100) surface model, on which 4-fold adsorption sites are numbered.

$$g_i(e)=\frac{1}{(\pi)^{1/2}\delta}\ p_i\exp\left[-\left(\frac{e-e_i}{\delta}\right)^2\right] \tag{2}$$

where, δ is an adjustable parameter affected by the number of K-points of the Brillouin zone, and p_i is a probability density at the energy level e_i. The summation runs over M band energy levels and the number of the K-points, L.

The COOP between two atoms in an oxygen molecule and those between oxygen and the surface nickel atoms are calculated by[23]

$$P_{AB}(e)=\sum_i g_i(e)P_{AB}(e_i) \tag{3}$$

where, $P_{AB}(e_i)$ is the overlap population between two bonding species at energy level e_i.

Core-electron binding energy shift. The binding energy of core-electron shifts upon the change of valence electron distribution in chemical or physical changes, since the core electron is partially shielded by outer valence electron distribution.[24-27] The shift is estimated theoretically using the valence potential model[27] in this work. This model is good enough for atoms such as oxygen, which have the K shell only in the core.

The binding energy shift of oxygen 1s level, ΔE, is obtained in reference to a standard state of the free molecule[27]

$$\Delta E=e\Delta\Phi \tag{4}$$

where, $\Delta\Phi$ is the difference of the valence potentials, and the valence potential, Φ, is calculated by[24,27]

$$\Phi=-2\sum_{i\neq core}<\phi_i|1/R_A|\phi_i>+\sum_{A\neq B}Z_B/R_{AB} \tag{5}$$

Here, R_A is the distance of the ith valence electron from the nucleus A, Φ_i is the wave function of the valence electron and summation runs over all the doubly occupied molecular orbitals. The second term is a potential energy due to the effective nuclear charge Z_B of the neighbouring atoms at R_{AB}.

Results and Discussion

Dissociative Adsorption. The DOS and the COOP are calculated varying the vertical distance of oxygen molecule from the 4-fold site of the nickel model surface. For the Ni(100) surface, a square lattice with 2.49 Å for Ni-Ni separation is used.[28] And the calculation is made with a 25 K

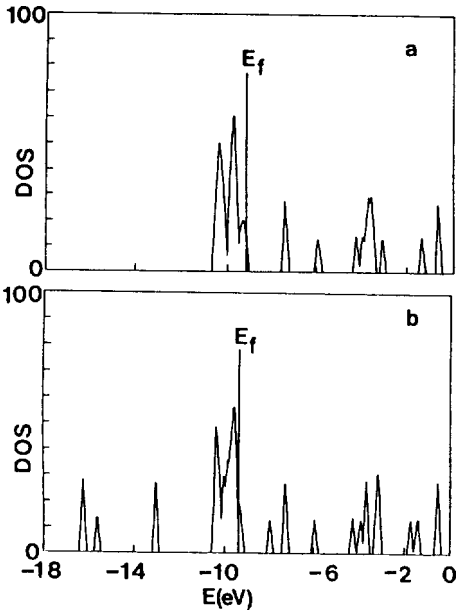

Figure 2. Total DOS of (a) Ni(100) surface, and (b) Ni(100)-O_2 system. Oxygen atom is adsorbed right on the 4-fold site, the vertical distance $R_\perp$ from the Ni(100) surface to oxygen being 1.66 Å. (Ref. 29-32).

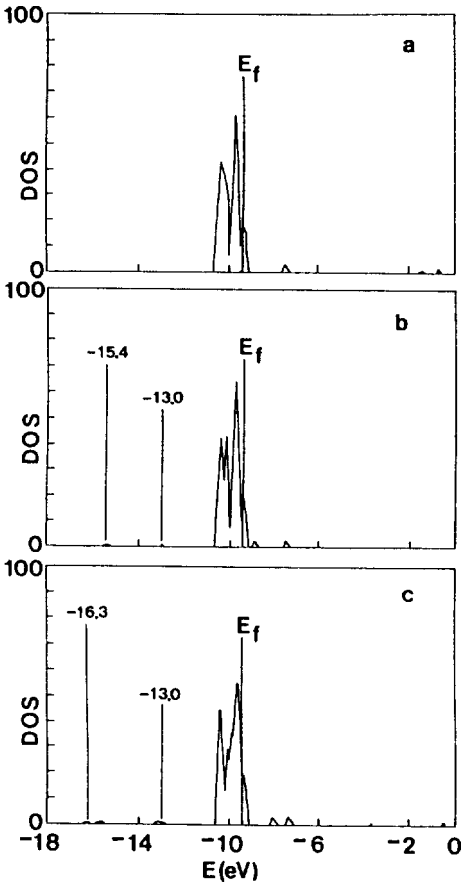

Figure 3. Projected DOS of total Ni-d; (a) $R_\perp=\infty$, (b) $R_\perp=2.0$ Å, and (c) $R_\perp=1.5$ Å. The numbers in the figures are the energy levels.

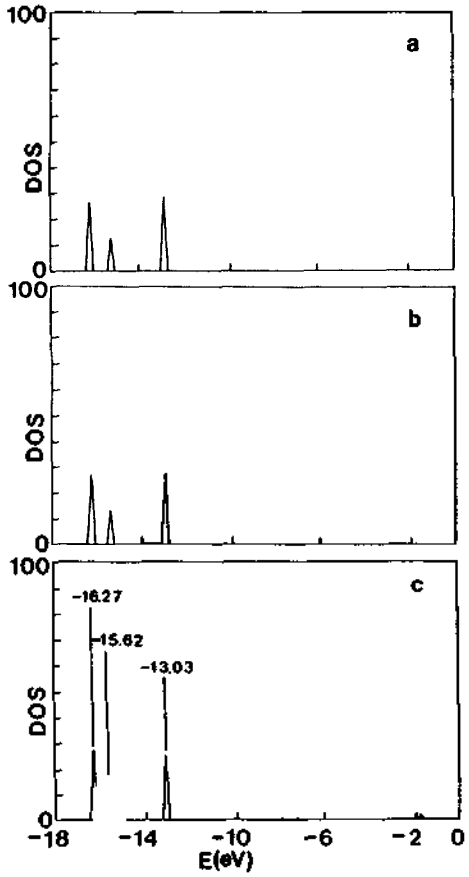

Figure 4. Projected total DOS of O_2; (a) $R_\perp = 2.5$ Å, (b) $R_\perp = 2.0$ Å, and (c) $R_\perp = 1.5$ Å. The numbers in the figure are the MO energy levels of O_2.

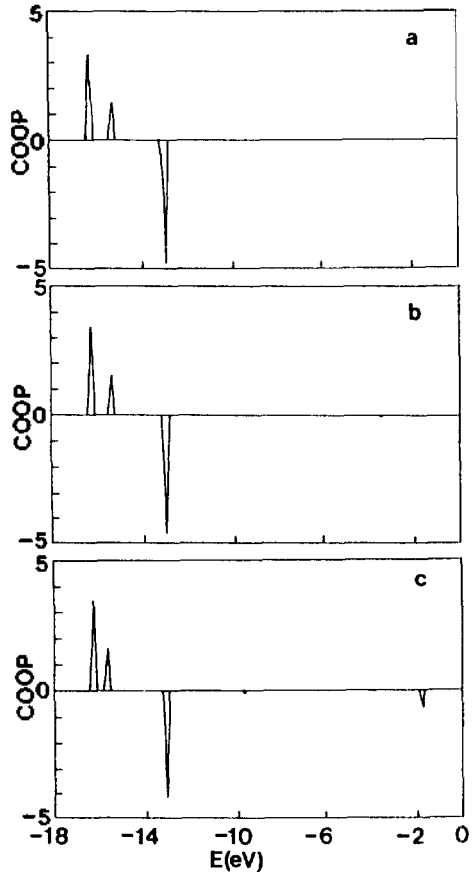

Figure 5. COOP of O_2 on the Ni(100) surface at (a) $R_\perp = 2.5$ Å, (b) $R_\perp = 2.0$ Å, and (c) $R_\perp = 1.5$ Å. The overlapping population of antibonding $1\pi_g$ decrease as the molecule approaches to the surface.

points set of the corresponding Brillouin zone. It is known that the small unit cell simplication is sufficient in estimating the surface-adsorbate interactions and the electronic nature of the surface rather than using the whole model surface.[17] For the adsorption system a unit containing 4 Ni atoms and one oxygen molecule is used to calculate the band of the oxygen molecule adsorbed on the Ni(100) surface. The total DOS of the adsorption system, the projected DOS of Ni-*d*, and the O_2 calculated are shown in Figure 2, 3, and 4, respectively.

It can be seen that new peaks appear at −15.4 eV and −13.0 eV in the *d*-DOS spectrum as the vertical distance approaches to 2.0 Å from the infinity, and another new peak at −16.3 eV as the vertical distance approaches more closely to 1.5 Å. It is found that the closer the oxygen molecule approaches to the nickel surface, the more *d*-DOS peaks appear at the low energy region in general. It is noted also that DOS at −13.0 eV increases notably as the vertical distance is decreased to 1.5 Å.

The COOP between two oxygen atoms in a molecule is calculated varying the vertical distance, and the results are shown in Figure 5. The positions of the peaks of the COOP between two oxygen atoms are also tabulated with their intensities in Table 1. It can be seen that the intensity of the COOP corresponding to the antibonding $1\pi_g$-orbital decreases and new COOP appear in the energy region heigher than

Table 1. The COOP between two oxygen atoms in a O_2 molecule on Ni(100) surface

	Position (eV)			Intensity of COOP (e)		
	$3\sigma_g$	$1\pi_u$	$1\pi_g$	$3\sigma_g$	$1\pi_u$	$1\pi_g$
Free O_2	−16.27	−15.13	−13.01	3.41	1.49	−4.72
$R_\perp = 2.0$ Å	−16.27	−15.41	−12.96	3.40	1.56	−4.66
$R_\perp = 1.5$ Å	−16.27	−15.62	−13.03	3.47	1.59	−4.23

−10.0 eV as the vertical distance becomes shorter. It is noted that the new COOP peaks in the heigher energy region correspond to the Ni *d*-DOS. The positional coincidence of the two COOP peaks is an indication of the interaction between the oxygen molecule and the nickel surface.

The COOP between the oxygen and nickel confirms further the interaction between the oxygen and the nickel surface as can be seen in Figure 6.

The peaks of Ni-O COOP show bonding in the lower energy region and antibonding in the heigher energy region. Especially, it is noticeable that the intensity of the bonding COOP at −13.1 eV increases very strongly compared to other peaks with the decreasing vertical distance. The position of this peak coincides with that of the antibonding $1\pi_g$-

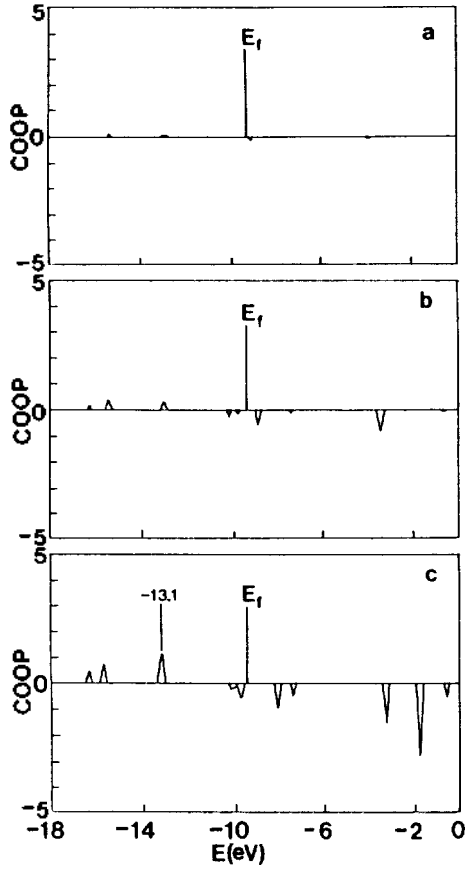

Figure 6. The COOP between Ni and O in Ni(100)-O_2 system; (a) $R_\perp = 2.5$ Å, (b) $R_\perp = 2.0$ Å, and (c) $R_\perp = 1.5$ Å. The Ni-O bonding increase as the $R_\perp$ becomes shorter.

Table 2. Overlap population between two atoms

	Ni-O	O-O
Free O_2		0.79
$R_\perp = 2.0$ Å	0.01	0.45
$R_\perp = 1.5$ Å	0.06	0.47

orbital of the oxygen molecule and also that of *d*-DOS of the nickel atoms as shown in Figure 2. These coincidences are an indication of strong interaction between O_2 $1\pi_g$-orbital and Ni *d*-orbital. The interaction is well agreed further with the atomic population calculations shown in Table 2. The overlap populations between the nickel and the oxygen atoms increase while those between the two oxygen atoms decrease with the decreasing vertical distance. This is an indication of increasing Ni-O intreaction at the expense of O-O interaction to result in a dissociative adsorption of oxygen on nickel surface. The weakening of the $1\pi_g$-orbital intensity of COOP with the decreasing vertical distance $R_\perp$ is another proof which support the dissociative adsorption. The weakening of the O-O bond results from the transfer of Ni *d*-electron to the partially filled $1\pi_g$-orbital.

The electron densities of various orbitals in oxygen molecule and nickel surface are tabulated in Table 3, along with their changes due to the interaction between both species. The difference, $\Delta d\pi$ and $\Delta d\delta$ are -0.04 and -0.49, respectively, showing the relatively large contribution of Ni $d\delta$ (or $d_{x^2-y^2}$ and d_{xy}) electrons and Ni $d\pi$ (or d_{xz} and d_{yz}) electrons as shown in Figure 7. Contrary to these differences, the interaction with $d\sigma$ (or d_{z^2}) is relativerly small as a consequence of the adsorption of oxygen on the 4-fold site. It can be

Table 3. Electronic structures of the oxygen and the Ni(100) Surface

O_2			Ni(100) surface						
Electron densities of free O_2			Electron densities of Ni(100) surface						
$3\sigma_g$	$1\pi_u$	$1\pi_g$	*s*	$p\sigma$	$p\pi$	$d\sigma$	$d\pi$	$d\delta$	E_F(eV)
2.00	4.00	2.00	0.21	0.02	0.01	1.90	4.00	3.87	−9.28
Electron densities of chemisorption system									
$3\sigma_g$	$1\pi_u$	$1\pi_g$	*s*	$p\sigma$	$p\pi$	$d\sigma$	$d\pi$	$d\delta$	E_F(eV)
1.93	3.71	3.88	0.22	0.02	0.01	1.94	3.96	3.38	−9.38
Electron density change									
$\Delta 3\sigma_g$	$\Delta 1\pi_u$	$\Delta 1\pi_g$	Δs	$\Delta p\sigma$	$\Delta p\pi$	$\Delta d\sigma$	$\Delta d\pi$	$\Delta d\delta$	ΔE_F(eV)
−0.07	−0.29	1.88[a]	0.01	0.00	0.00	0.04	−0.04	−0.49	−0.10
Overlap population									
	Ni-O					O-O			
	0.01					0.43			

Electron density changes are the differences between the system of O_2 and Ni(100) surface infinitely separated and the system of O_2 and Ni(100) surface interacting in an adsorbed state. [a]This is the total electron density in two degenerate $1\pi_g$ orbitals, that is, each $1\pi_g$ orbitals gain 0.94e.

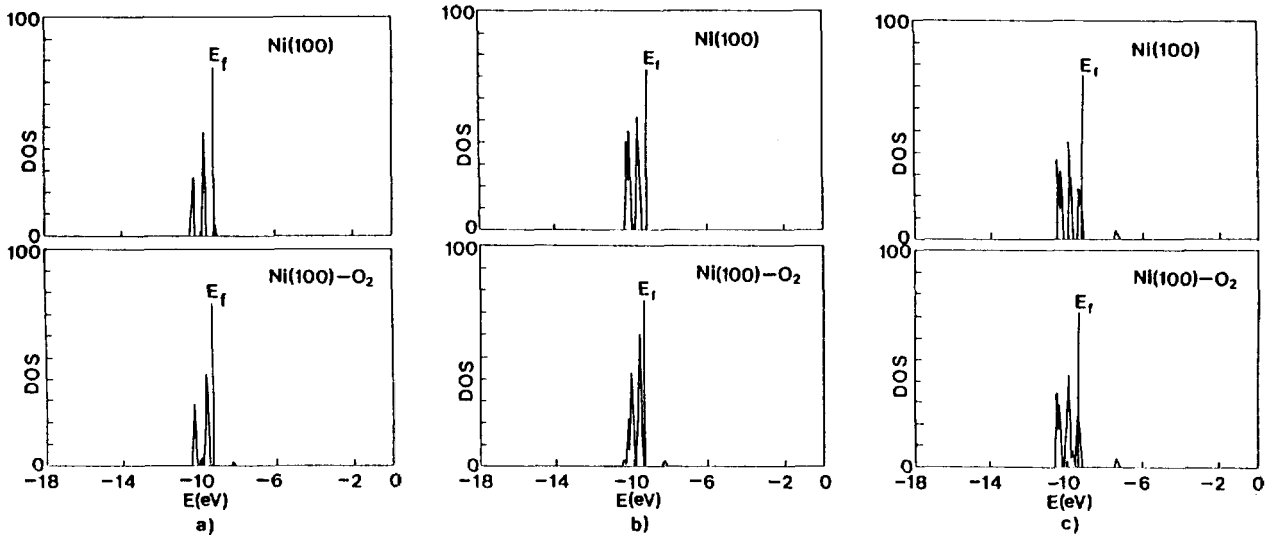

Figure 7. Projected DOS of d in Ni(100) and Ni(100)-O_2 system at $R_\perp = 1.66$ Å; (a) $d\sigma$ (or d_{z^2}), (b) $d\pi$ (or d_{xz}, d_{yz}) and (c) $d\delta$ (or $d_{x^2-y^2}$, d_{xy}).

Table 4. The minimum potential energy between the oxygen and the nickel atoms and their separation

Position	$R_\perp$ (Å)	E (eV)
2-fold bridge	1.73	−76.6
3-fold hole (edge)	1.66	−76.1
4-fold hole	1.66	−76.7

concluded that the $d\delta$ and $d\pi$ electrons are transferred to $1\pi_g$ antibonding orbitals of oxygen molecule, effecting the dissociation of the adsorbing oxygen molecule.

Binding Energy Shift of Oxygen Core Electrons. The minimum potential energies and the vertical separations of the oxygen atom above the model cluster surface are also listed in Table 4.

The result of calculation shows that oxygen atom can be adsorbed on the 4-fold sites as well as on the 2-fold bridge sites, whereas the experimental results favor the 4-fold sites.[10] Meanwhile, the potential energy of oxygen atom interacting with the nickel atoms on the 4-fold site is calculated extending the number of nickel atoms from 4 to 6, 12, and 24, in order to estimate the effect of the 2nd and the further nearest neighbor nickel atoms. The effect on the potential is found to be less than 0.1%, confirming the experimental findings that the oxygen interacts mainly with the 4 nearest nickel atoms.[11] The core electron binding energy shift of the oxygen atom adsorbed on the site 5 in Figure 1 is also calculated using Eq. (5) by the EHT method under various atmosphere of neighboring oxygen atoms in order to estimate any effect of neighbouring adsorbed oxyygen atoms, and the results are shown in Table 5. The values in the second column of the table is for the oxygen atoms adsorbed at the initial stage prior to any ordered structure formation. The 3rd column is for $p(2\times2)$ structure, and all the remaining columns are the results for the $c(2\times2)$ structure. The Table 5 indicates that the 1s binding energy shift of oxygen atoms adsorbed on the 4-fold site is unaffected by the 2nd nearest neighbor oxygen atoms and is about 11.5 eV independent almost of their geometrical arrangement on the model surface.

Table 5. Binding energy shift of 1s electron of oxygen adsorbed on the center of the model surface

Structure	Submono -layer	$p(2\times2)$	$c(2\times2)$	$c(2\times2)$	$c(2\times2)$	$c(2\times2)$
adsorbed atomic number	2,3,5	1,2,3 4,5	5,6,7 8,9	3,5,6 7,8,9	2,3,5,6 7,8,9	1,2,3,4,5 6,7,8,9
Φ (eV)	−18.53	−18.61	−18.55	−18.30	−18.28	−18.41
ΔBE (eV)	11.39	11.31	11.37	11.62	11.64	11.51

$\Delta BE = \Phi - \Phi_\infty$ (in free O_2), $\Phi_\infty = 29.92$ eV.

Table 6. Binding energy shift of O 1s electron at edge site and excess site

Structure	Edge (1,2,3,4)	Excess (10)	Excess (10,11)
adsorbed atomic number	1,2,3,4,5 6,7,8,9	1,2,3,4,5 6,7,8,9,10	1,2,3,4,5,6, 7,8,9,10,11
Φ (eV)	−16.92	−19.25	−19.36
ΔBE (eV)	13.00	10.67	10.56

Numbers in the parenthesis are adsorbed oxygen atoms in Fig. 1.

The binding energy is calculated for the atoms adsorbed on the edge of the model surface and for those interstitially adsorbed in excess of the ordered structure and the results are shown in Table 6. The small shift shown by the interstitially adsorbed oxygen atom can be attributed to the fact that most of the valence electrons of the nearby nickel atoms have been transferred to other orderly adsorbed oxygen atoms.

In this work, three different values are obtained for the O 1s binding energy shift, 10.6, 11.5, and 13.0 eV. These

Table 7. The experimental binding energy (BE) and binding energy shift (ΔBE) of O 1*s* electron on Ni surface (eV)

	BE	ΔBE	State of O
Free Oxygen Atom[33]	543.1± 0.2	0	
Kim[5]	531.3	11.8	Ni_2O_3
	533.1	10.0	NiO_{ad}
Evans[6]	529.8	13.3	
	531.0	12.1	
Brundle[7]	529.5	13.6	oxide Form
	531.4	11.7	Ni_2O_3
	532.2	10.9	Precursor
	533.2	9.9	Submonolayer
Ahn[8]	529.7	13.4	Oxide
	530.2	12.9	Dissociative
	531.3	11.8	Non-stoichiometry

Table 8. EHT parameters

	ζ_s	H_s	ζ_p	H_p
Ni	1.400	−7.635	0.860	−3.99
O	2.895	−32.48	2.475	−14.90

ζ_{d1}	H_d	C_1^a	ζ_{d2}	C_2^a
5.700	−11.9	0.5705	1.68	0.6317

[a]Coefficients of double zeta expansion.

values lie in a very close proximity to the XPS measurements.[5-8] Some of the O 1*s* shifts on nickel surface, reported by some investigators, are quoted in Table 7 for reference. Definite proof can not be obtained beyond the encouragement in this work which will ascribe the dubious 531.3 eV O 1*s* peak (11.8 eV in ΔBE) either to non-stoichiometric excess or to Ni_2O_3. Further necessary work is in progress with other low index surfaces.

Acknowledgement. This work is supported financially by the Ministry of Education, through the Basic Research Institude program.

Appendix

All the calculations are made with the tight-binding EHT type, using PC/386. The program used in this work is obtained by converting the QCPE571(VAX version) into the PC version. The coulomb integral H_{ii} in the band calculation are obtained by the charge iteration method.[34] The iteration parameters *A*, *B* and *C* are taken from reference 35. The ionization potential H_{ii} in the EHT calculation are adjusted to bring the calculated atomic separations in Ni-O system close to the experimentally observed values (Table 8). The Hückel constant used in this work is 2.25 and the Ni-Ni and O-O distances are 2.49 Å[28] and 1.21 Å[36] respectively. All other parameters used in this work is taken from the table given by Hoffmann.[16]

Reference

1. Bielanski, B.; Majbar, M. J. *Catalysis* **1973**, *25*, 398.
2. Dyrek, K. *Advan. Mol. Relaxation Interaction Processes*; **1973**, *5*, 211.
3. Tsyganenko, A. A.; Rodionova, T. A.; Filimonov, V. N. Reaction Kinet., *Catalysis Letters* **1979**, *11*, 113.
4. Hegde, M. S; Ayoob, D. *Surf. Sci.* **1986**, *173*, 635.
5. Kim, K. S.; Winograd, N. *Surf. Sci.* **1974**, *43*, 625.
6. Evans, S.; Pielaszek, J.; Thomas, J. M. *Surf. Sci.* **1976**, *56*, 644.
7. Brundle, C. R.; Hopster, H. *J. Vac. Sci. Technol.* **1981**, *18*, 663.
8. Ahn, W. S.; Lee, K. S.; Ham, K. H.; Lee, S. B.; Boo, J. H. *Bull. Kor. Chem. Soc.* **1988**, *9*(1), 32.
9. Arnaud, Y. P. *Appl. Surf. Sci.* **1992**, *62*, 21.
10. Stöhr, J.; Jäger, R; Kendelewicz, T. *Phys. Rev. Lett.* **1982**, *49*, 142.
11. Rahman, T. S.; Black, J. E.; Mills, D. L. *Phys. Rev. Lett.* **1981**, *46*, 1469.
12. Antonongeli, F.; Crescenzi, M. D.; Bellini C.; Rosei, R. *Phys. Rev. Lett.* **1983**, *50*, 1949.
13. Anderson, A. B. *J. Chem. Phys.* **1974**, *61*, 4545.
14. Blyholder, G. *J. Phys. Chem.* **1964**, *68*, 2772.
15. Whangbo, M. H.; Hoffmann, R. *J. Am. Chem. Soc.* **1978**, *100*, 6093.
16. Saillard, J. Y.; Hoffmann, R. *J. Am. Chem. Soc.* **1984**, *106*, 2006.
17. Sung, S. S.; Hoffmann, R. *J. Am. Chem. Soc.* **1985**, *107*, 578.
18. Tremel, W.; Hoffmann, R. *J. Am. Chem. Soc*, **1987**, *109*, 124.
19. Whangbo, M. H.; Hoffmann, R.; Woodward, R. B. *Proc. R. Soc. Lond.* **1979**, *A366*, 23.
20. Albright, T. A.; Burdett, J. K.; Whangbo, M. H. *Orbital Interaction in Chemistry*; Wiley: New York, 1985.
21. Hoffmann, R. *Solid and Surface: A Chemist's View of Bonding in Extended Structure*; VCH Publish Inc.: **1988**.
22. Muetterties, E. L.; Rhodin, T. N.; Band, Elliot.; Brucker, C. F.; Pretzer, W. R. *Chem. Rev.* **1979**, *79*, 91.
23. Canadell, E.; Whangbo, M. H. *Chem. Rev.* **1991**, *91*, 965.
24. Schwartz, M. E. *Chem. Phys. Lett.* **1970**, *6*(6), 631.
25. Schwartz, M. E. *J. Chem. Phys. Lett.* **1970**, *7*(1), 78.
26. Davis, D. W.; Shirley, D. A. *Chem. Phys. Lett.* **1972**, *15*(2), 185.
27. Ghosh: P. K. *Introduction to Photoelectron Spectrosocopy*; John Wiley & Sons Inc. 1983; p 63.
28. Wong, Y. T.; Hoffmann, R. *J. Phys. Chem.* **1991**, *95*, 859.
29. Anderson, A. B. *J. Chem. Phys.* **1977**, *66*(5), 217.
30. Allen, V. M.; Jones, W. E.; Pacey, P. D. *Surf. Sci.* **1989**, *200*, 193.
31. Castejon, H.; Hernandez, A. J.; Ruette, F. *J. Phys. Chem.* **1988**, *92*, 4970.
32. Burdett, J. K.; Czech, P. T.; Fässler, T. F. *Inorg. Chem.* **1992**, *31*, 129.
33. Siegbahn, K. *et al. ESCA Applied to Free Molecules*; North-Holland Publishing Company: Amsterdam-London, 1969; p 72.

34. Ballhausen, C. J.; Gray, H. B. *Molecular Orbital Theory*; W. A. Benjamin Inc.: New York, 1964; p 120.
35. McGlynn, S. P.; Vanquickenborne, L. G.; Klinoshita, M.; Caroll, D. G.*Introduction to Applied Quantum Chemistry*; Hott, Rinehart and Winston Inc.: New York, 1972; p 423.
36. Wells, A. F. *Structural Inorganic Chemistry*; Clarendon Press.: Oxford, 1984; p 498.

Spectroscopic Properties and Ligand Field Analysis of Tris[(±)-*trans*-1,2-cyclohexanediamine]chromium(III) Chloride[1]

Jong-Ha Choi

Department of Chemistry, Andong National University, Andong 760-749
Received September 3, 1993

The low temperature luminescence and excitation, room-temperature UV-visible and infrared spectra of $[Cr(\pm)chxn_3]Cl_3$ (chxn=*trans*-1,2-cyclohexanediamine) have been measured. It is found that the zero-phonon line in the excitation spectrum splits into two components by 47 cm^{-1}. The eight electronic transitions due to spin-allowed and spin-forbidden are assigned. As expected, nitrogen atoms of chxn ligand have strong σ-donor properties toward chromium(III). The positions and splittings of sharp-line transitions are analyzed as a function of the Cartesian bite (α) and twist (β) angles to predict the metal-ligand geometry.

Introduction

Sharp-line electronic spectroscopy has provided a powerful tool for extracting geometric informations.[2] The sharp-line electronic transitions are very sensitive to the exact bond angles around the metal. Thus it is possible to obtain a structural information from sharp-line electronic spectrum quickly without a full X-ray structure determination.

Luminescence, absorption and excitation spectroscopic studies of chromium(III) complexes began with hexacoordinated nitrogen complexes, because their intensities tend to be quite strong. A number of such complexes have already been investigated.[3] The spectroscopic properties of CrN_6 complexes are very similar, although the photochemical quantum yields vary considerably. Wasgestian and Gowin have reported photosubstitution quantum yields of chromium(III) complexes with CrN_6 skeletons in acid solution.[4]

When a cyclohexane ring is fused with a five-membered chelate ring, the chelate ring is not able to exhibit the puckering motion. Hence, it was possible to separate and characterize eight possible isomers of $[Cr(chxn)_3]^+$ ion.[5] The X-ray crystal structure of *lel*$_3$-$[Cr(chxn)_3](NO_3)_3 \cdot 3H_2O$ has been studied.[6] The electrostatic and hydrophobic interactions in the ion associations between the $[Cr(chxn)_3]^+$ ion and the sulfonate anions have been investigated.[7] The absorption and circular dichroism spectra in the spin-forbidden transitions have also been reported.[8]

We have measured the 77 K luminescence and 12 K excitation, and room-temperature UV-visible and infrared spectra of $[Cr(\pm)chxn_3]Cl_3$. In this paper we describe its spectroscopic and ligand field properties. The relationship between the metal-ligand geometry and the sharp-line electronic transitions is discussed.

Experimental Section

Synthesis. All chemicals were reagent grade quality and used without further purification. Tris[(±)-*trans*-1,2-cyclohexanediamine]chromium(III) chloride was prepared according to Pederson's method[9] by use of racemic *trans*-1,2-cyclohexanediamine. The compound was recrystallized three times for spectroscopic measurements.

Measurements and Computations. The room-temperature absorption spectrum in aqueous solution was recorded with a Hewlett-Packard Model 8451A diode array spectrophotometer. The far-infrared spectrum was recorded with a Bruker 113 V instrument on a microcrystalline sample pressed in to a polyethylene pellet. These measurements were done at room-temperature by Dr T. Schönherr at the University of Düsseldorf. The mid-infrared spectrum was recorded with a Mattson 2020 Galaxy FT-IR spectrometer on a KBr pellet. The luminescence spectrum was measured at 77 K on a Spex Fluorolog-2 spectrofluorometer as previously described.[3c]

The excitation spectrum of $[Cr(\pm)chxn_3]Cl_3$ at 12 K was measured by monitoring the luminescence intensity of the vibronic sideband at 709 nm. The light from an EG & G PAR Dyescan nitrogen laser-pumped dye laser was focused on a microcrystalline sample mounted with conductive grease on the cold head of an Air Products Displex CSA-202E cryostat. The emitted light was dispersed by a Spex Double 220 mm monochromator with 0.5 mm slits. The output from a cooled Hamamatsu R928 photomultiplier was passed to an SRS boxcar integrator, triggered by a fraction of the laser pulse passed to a fast photodiode. The excitation wavelength was calibrated by using four neon optogalvanic resonance points. The excitation spectrum was corrected for the laser